Simple and Compact Balanced Bandpass Filters Based on Magnetically Coupled Resonators

Armando Fernández-Prieto, Aintzane Lujambio, Jesús Martel, *Senior Member, IEEE*, Francisco Medina, *Fellow, IEEE*, Francisco Mesa, *Fellow, IEEE*, and Rafael R. Boix, *Member, IEEE*

***Abstract*—A simple strategy is proposed to design differential-mode bandpass filters with good common-mode (CM) rejection using simple resonators. Specifically, the CM rejection is enhanced by using conventional open-loop resonators as well as folded stepped-impedance resonators without the addition of printed or lumped elements along the symmetry plane of the filter or the use of defected ground solutions. The novelty of the present proposal is that a good CM rejection is achieved by the use of magnetic coupling instead of the more commonly employed electrical coupling. Magnetic coupling inherently yields poorer CM transmission as requested by good differential filters. The resonators, due to their geometrical simplicity, can easily be cascaded to implement high-order filters. The use of simple geometries also simplifies the design methodology and makes final tuning based on electromagnetic simulation simpler or unnecessary.**

***Index Terms*—Balanced differential filters, common-mode (CM) suppression, magnetic coupling, stepped-impedance resonators.**

I. Introduction

THE USE of balanced differential circuit architectures [1] for both digital high-speed electronics and analog microwave circuits has become very popular in recent years due to their high degree of immunity to environmental noise and electromagnetic interference, as well as their good electromagnetic compatibility performance when compared with single-ended configurations. This trend has pushed on the research on differential versions of classical single-ended passive components. Some examples of this kind of research are power dividers and combiners [2]–[5], diplexers [6], or passive equalizers [7]. Nevertheless, common-mode bandstop filters (CM-BSFs) and differential-mode bandpass filters (DM-BPFs) are by far the components that have received more attention [8] in this frame. A few typical examples of CM-BPFs implemented in printed circuit technology can be found, for instance, in [8]–[13]. These structures are designed to reject the common-mode (CM) signal over a wide frequency band, whereas the insertion loss (IL) for the differential signal is kept as low as possible (through good matching and low losses) from dc to the highest frequency of interest. Our attention in this work will be focused on DM-BPFs. These components are designed so that they behave as standard single/multiple BPFs for the differential signal (low IL at the desired frequency bands and strong rejection in the out-of-band regions) while also showing strong rejection of the CM signal over the differential passband(s) and around them.

Many works dealing with DM-BPFs have been published in the open literature during the last decade, and thus a wide variety of possible implementations is available today for single-band, dual-band, narrowband, or wideband applications. Some recent illustrative examples are: narrowband BPFs based on closed-loop resonators [14], dual-band differential filters based on asymmetrical coupled lines [15], compact narrowband filters based on defected ground structure (DGS) [16], and wideband differential filters based on branch $\lambda/4$ coupled lines [17] or on modified branch lines [18]. Differential filters based on surface integrated waveguide technology have also been reported [19].

Most of these filters exhibit a symmetry plane that behaves as an electric/magnetic wall depending on the symmetry (differential/common, odd/even) of the excitation. The structure resulting of forcing an electric wall (short circuit) at the symmetry plane should fulfill the specs of the desired differential filter. The CM response can then be derived from the same geometry after enforcing the symmetry plane to be a magnetic wall (open circuit). If the desired level of CM rejection is not directly provided by the CM equivalent structure, electrical components can be added along the symmetry plane to improve the CM response without affecting the differential-mode (DM) response. This strategy suggests that DM filters can be derived from their single-ended counterparts after introducing a symmetry plane by specular reflection or by choosing a symmetrical version of the filter. Actually, many of the DM-BPFs described in the literature are symmetrical structures of this class [15], [20]–[26].

One of the simplest filters that can be designed (provided a narrow passband suffices for the application) is based on the use of coupled open-loop resonators, which is, in fact, the starting structure considered in [20]. If a more compact version of the same kind of filter is desired, folded stepped-impedance resonators (FSIRs) could be used instead of the open-loop resonators. However, the straightforward implementation of the differential version of the basic second-order filter based on this topology does not yield good CM rejection [20]. As mentioned

Manuscript received November 07, 2014; revised February 05, 2015 and March 25, 2015; accepted March 29, 2015. Date of publication May 01, 2015; date of current version June 02, 2015. This work was supported by the Spanish Ministry of Economy and Competitiveness with European Union FEDER Funds under Contract TEC2010-16948, Contract TEC2013-41913-P, and Contract Consolider EMET CSD2008-00066, and by the Spanish Junta de Andalucía under Project P12-TIC-1435.

A. Fernández-Prieto, A. Lujambio, F. Medina, and R. R. Boix are with the Faculty of Physics, Department of Electronics and Electromagnetism, University of Sevilla, 41012 Seville, Spain (e-mail: medina@us.es).

J. Martel is with the Department of Applied Physics II, ETSA, 41012 Seville, Spain.

F. Mesa is with the Department of Applied Physics I, ETSII, 41012 Seville, Spain.

Color versions of one or more of the figures in this paper are available online at http://ieeexplore.ieee.org.

Digital Object Identifier 10.1109/TMTT.2015.2424229

before, this drawback is usually overcome by adding tuning elements along the symmetry plane, which do not affect the DM operation too much, but improve the CM rejection performance. In this paper, it will be shown that, in the case of two resonators (second-order filters), this is not necessary if magnetic coupling is employed instead of the commonly used electric coupling. Magnetic coupling can easily be achieved by simply rotating the resonators 180° with respect to an axis perpendicular to AA'. For a given level of required coupling, the magnetic version gives place to a larger separation between the resonators. However, even though magnetic coupling provides the interaction mechanism for DM operation, the resonators are still electrically coupled under CM excitation. The level of electric coupling in this case is much lower than the one involved in the original structure based on electrical coupling for both DM and CM excitations, thus giving place to weak CM transmission. However, if magnetic coupling is used in the design of the differential response, the excitation of the filter has to be carried out through capacitive coupling since, otherwise, the appropriate values of external quality factor cannot be achieved. Fortunately this is not a problem if planar interdigitated capacitors are used when tight feed coupling is required. A very good performance can be achieved with this simple strategy, which is experimentally demonstrated here for two second-order demonstration filters based on open-loop resonators and FSIRs. Two key features of the present approach are: 1) no additional tuning has to be done to improve CM rejection and 2) increasing the order of the filter is a trivial task in comparison with implementations based on complex resonator geometries since the basic resonator is geometrically very simple.

This paper is organized as follows. Section II presents the design of a simple narrowband DM-BPF based on electrically coupled open-loop resonators with symmetrically taped excitation, and its performance is compared with the magnetically coupled version to show the superiority of the last one with respect to CM rejection requirements. A similar study is carried out in Section III for the second-order filters based on electrically coupled and magnetically coupled FSIRs. A fourth-order filter based on the use of four inline FSIRs including one magnetically coupled pair is finally shown in Section IV.

II. Open-Loop Coupled-Resonator Balanced Bandpass Filters

A. Conventional Case: Electrically Coupled Resonators

The layout of the straightforward implementation of a balanced bandpass filter based on two electrically coupled open-loop resonators is shown in Fig. 1. This is the unloaded version of the structure analyzed in [20]. The design of the differential response can be carried out following the procedure described in [27] for coupled-resonator filters, where the involved resonators would be the ones in Fig. 1 with a virtual ground at the AA' plane. The inter-resonators coupling factor, M, and the external quality factor, Q_e, required to obtain the desired fractional bandwidth, Δ, is given, in general, by the following expressions:

$$M_{i,i+1} = \frac{\Delta}{\sqrt{g_i g_{i+1}}}, \qquad \text{for } i = 1, \ldots, n-1 \tag{1}$$

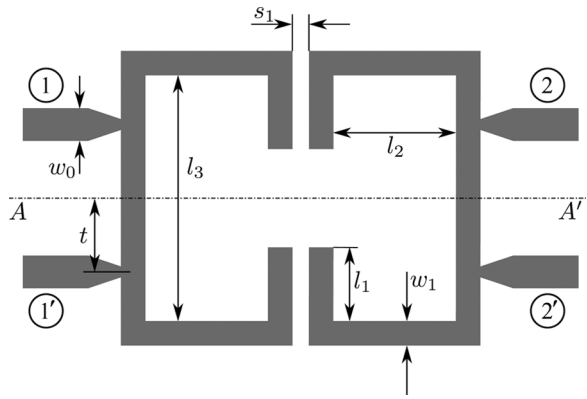

Fig. 1. Layout of an electrically coupled open-loop balanced bandpass filter (no attention is paid to CM performance). The final dimensions of the designed second-order Butterworth filter ($f_0^d = 2.45$ GHz, $\Delta = 10\%$) are $l_1 = 2.5$ mm, $l_2 = 8.75$ mm, $l_3 = 16.9$ mm, $w_0 = 2.53$ mm, $w_1 = 0.8$ mm, $t = 2.435$ mm, and $s_1 = 0.53$ mm.

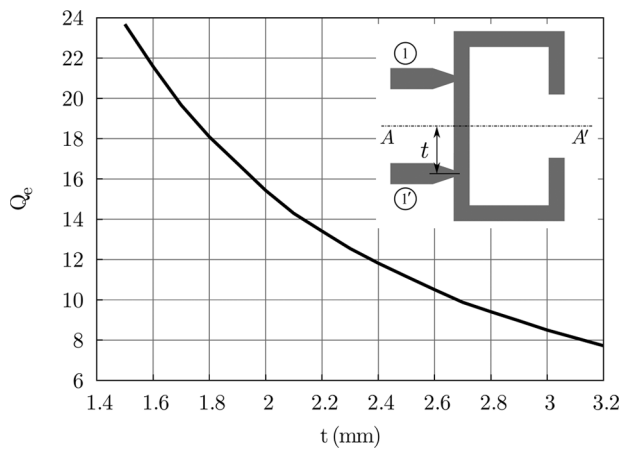

Fig. 2. DM external quality factor (Q_e) versus t obtained through the computation of S_{11}^{dd} for the structure in the inset. ADS Momentum has been used for the full-wave simulations.

$$Q_{e1} = \frac{g_0 g_1}{\Delta} \quad Q_{en} = \frac{g_n g_{n+1}}{\Delta} \tag{2}$$

where n is the filter order and $g_i (i = 1, \ldots, n-1)$ are the low-pass prototype element values for the filter response that are aimed to be implemented. The center frequency, f_0^d, is controlled by the length of the open-loop resonator, which has to be close to half the guided wavelength at such frequency.

As an example, the $n = 2$ Butterworth design with $f_0^d = 2.45$ GHz and $\Delta = 10\%$ is considered. For such design, $M_{12} = 0.071$ and $Q_{e1} = Q_{e2} = Q_e = 14$ are required. For the chosen substrate ($\varepsilon_r = 3.0, h = 1.016$ mm), the following resonator dimensions are selected: $l_1 = 2.5$ mm, $l_2 = 8.75$ mm, $l_3 = 16.9$ mm, and $w_1 = 0.8$ mm. The value of Q_e is mainly controlled by the tap distance t (see Fig. 1). The procedure reported in [27, Ch.7] can be followed to extract Q_e using a full-wave simulator (ADS Momentum [28] has been used here). The variation of Q_e with respect to t is plotted in Fig. 2. From this figure, the appropriate tap position leading to $Q_e = 14$ is found to be $t = 2.12$ mm. The coupling coefficient (M_{12}) is controlled by the gap distance between resonators, s_1. From the

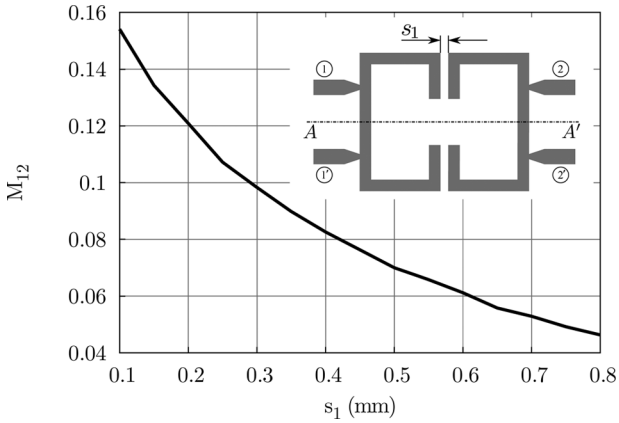

Fig. 3. DM coupling coefficient (M_{12}) as a function of the gap separation between adjacent resonators, s_1.

values of the two resonance frequencies, f_{p1} and f_{p2}, of the coupled open-loops shown in the inset of Fig. 3, the value of M_{12} is obtained using the formula [27]

$$M_{12} = \frac{f_{p1}^2 - f_{p2}^2}{f_{p1}^2 + f_{p2}^2}. \tag{3}$$

The design curve relating M_{12} to s_1 is shown in Fig. 3. From this figure, a gap distance of $s_1 = 0.5$ mm gives us the required value of $M_{12} = 0.071$. After a final fine tuning process, the definitive values for fabrication were $s_1 = 0.53$ mm and $t = 2.43$ mm. Finally, the 50-Ω microstrip characteristic impedance corresponds to $w_0 = 2.53$ mm.

The simulated and measured results for both DM and CM excitation for the filter shown in Fig. 1 are depicted in Fig. 4(a). A detail of the DM response is shown in Fig. 4(b), where a photograph of the fabricated prototype is also included. The simulated and measured results satisfy the required DM specs with reasonably low IL (0.81 dB measured at f_0^d). Unfortunately, a poor CM rejection level is found for this type of filters, as clearly indicated by the common-mode rejection ratio (CMRR) at f_0^d (around 14 dB). Most of the contributions that can be found in the literature try to improve this CM rejection by introducing some additional structures along the symmetry plane, AA', of the filter. When operating in CM, AA' behaves as a perfect magnetic wall (virtual open circuit), and thus any extra element introduced in the symmetry plane will influence the CM response. In contrast, the DM will not be affected by these new elements since AA' is an electric wall (virtual short circuit) in such case. Typical elements used to reduce CM transmission are lumped inductors and capacitors, $\lambda_g/2$ open-circuited stubs or DGSs.

In this paper we do not follow the above guideline of adding elements along the symmetry plane, which additionally makes the design process more difficult and might even preclude the use of these structures for high-order filter design. Instead, our proposal is to employ magnetic coupling rather than electric coupling in the design of the differential filter. Interestingly, this leads to more separate resonators that are weakly coupled under CM excitation, thus giving place to inherent low CM transmission. Although magnetic coupling has incidentally been introduced in some differential filter designs [14], [29], [30], [32], to the authors' knowledge, the relevance of this fact to suppress

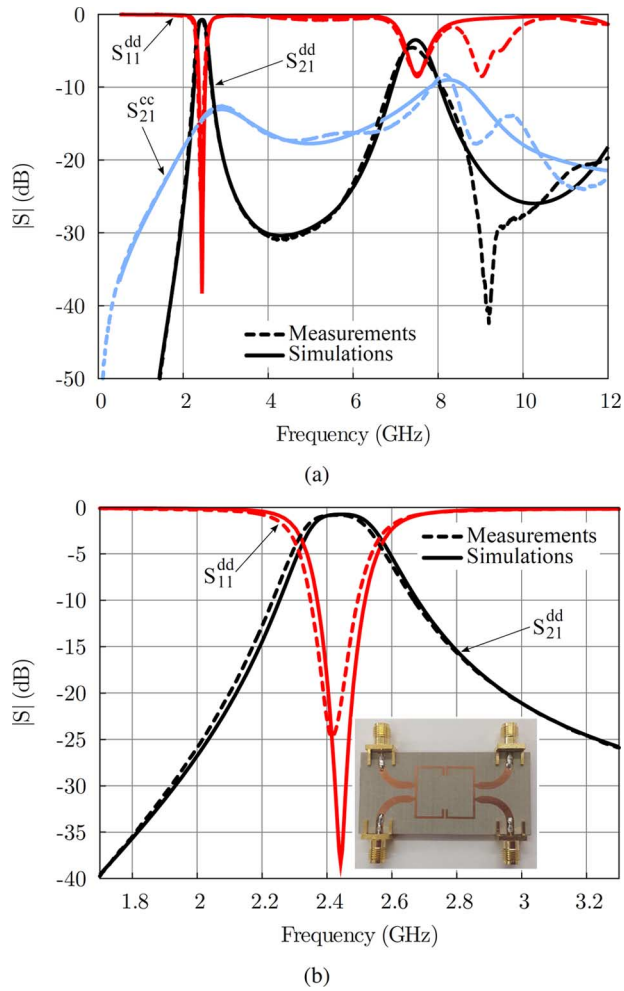

Fig. 4. (a) Simulated and measured DM and CM response of the conventional open-loop balanced bandpass filter of Fig. 1. (b) Detail of the differential passband including a photograph of the prototype.

CM transmission has not been exploited before. When electric coupling is used in the differential filter design, both CM and DM coupling levels are of the same order of magnitude. On the contrary, if magnetic coupling is used to achieve the required DM response, the associated level of electric coupling affecting CM operation can be, at least, one order of magnitude smaller (for typical values of the dielectric constant of the substrate).

B. Alternative Design: Magnetically Coupled Resonators

The layout of the magnetically coupled version of the filter reported in Section II-A is shown in Fig. 5. The new structure is obtained by rotating around an axis perpendicular to AA' 180° each of the electrically coupled resonators of Section II-A in such a way that the coupling between them is now mainly magnetic.

The same substrate, filter type, filter order, specs, and working frequency are used to illustrate the advantages of the new design. The same classical design procedure employed before can be followed for the new configuration. Therefore, the same values of M_{12} and Q_e are required. The main difference is that the excitation of the pair of resonators must now be of capacitive nature to be capable of implementing

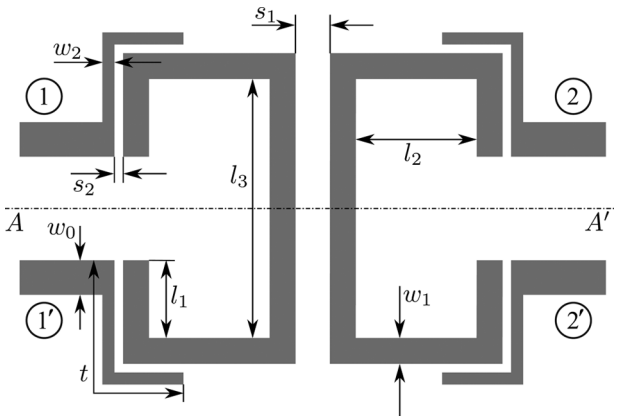

Fig. 5. Layout of a magnetically coupled open-loop balanced bandpass filter of second order. The final dimensions of the designed filter (same specs as in Fig. 1 are $l_1 = 4$ mm, $l_2 = 4.9$ mm, $l_3 = 16.9$ mm, $w_0 = 2.53$ mm, $w_1 = 0.8$ mm, $w_2 = 0.3$ mm, $t = 9$ mm, $s_1 = 1.6$ mm, and $s_2 = 0.1$ mm.

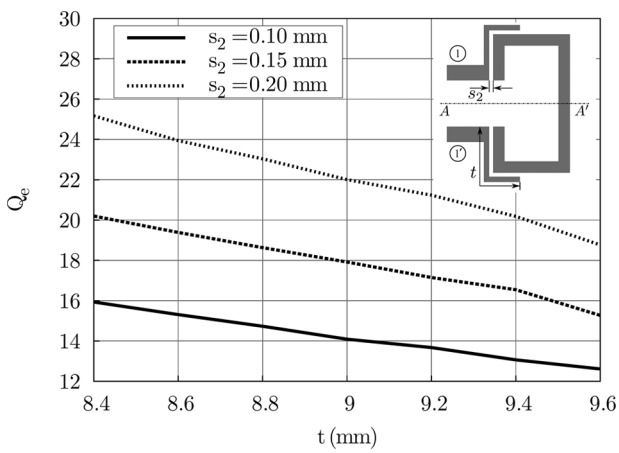

Fig. 6. DM external quality factor, Q_e, as a function of the length of the capacitive feeding lines, t, for several values of the separation s_2.

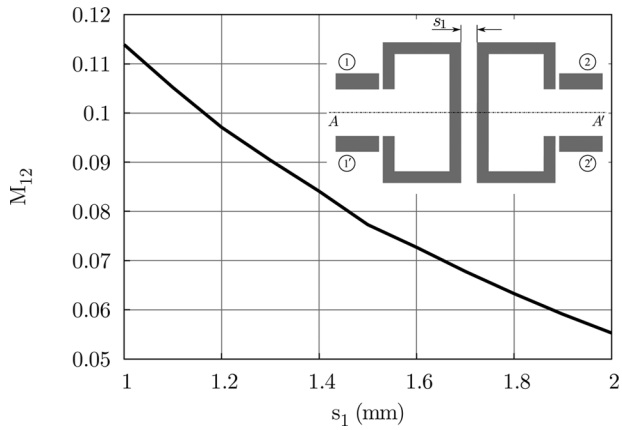

Fig. 7. Simulated DM coupling coefficient, M_{12}, versus the gap between the resonators, s_1, for the magnetically coupled open-loop resonators used in our design.

the required value of Q_e. This capacitive excitation makes the interaction with the resonators different and modifies the resonance frequency of the resonators. In order to bring the resonance frequency to the required value, the dimensions of the resonators have to be adjusted to the following values: $l_1 = 4$ mm, $l_2 = 4.9$ mm, $l_3 = 16.9$ mm, and $w_1 = 0.8$ mm. Note that, incidentally, the new filter is shorter than the previous one. Again, we can obtain design curves for Q_e and M_{12} similar to those in Figs. 2 and 3. These new curves are depicted in Figs. 6 and 7. The parameters that now control Q_e are the width, w_2, and length, t, of the capacitively coupled feeding lines and their separation to the resonator, s_2. We can choose w_2 within a wide range of values provided two conditions are fulfilled, which are: 1) t is short enough to neglect I/O coupling and 2) s_2 is wide enough to avoid problems related to fabrication tolerances. The chosen value, $w_2 = 0.3$ mm, fulfills both requirements. The other two parameters have been varied to obtain the design curves in Fig. 6. From Figs. 6 and 7, we extract the following dimensions to fulfill the filter specs: $s_1 = 1.6$ mm, $s_2 = 0.1$ mm, and $t = 9$ mm. Note that the feeding lines and the resonators have to be closely spaced to reach the required value of Q_e.

The final design has been simulated and a fabricated prototype has been measured. The results are plotted in Fig. 8 for both DM and CM excitations. The comparison of this response with one of the previous filters makes it apparent that CM noise suppression has been drastically improved; specifically, a measured value of CMRR ($@f_0^d$) equal to 40 dB has been obtained. This 26-dB improvement has been achieved without the addition of new elements that would have complicated the design process. As required, the DM response also has a reasonably good performance, although the measured IL is slightly worse in the new design (1.28 dB has been measured at the center frequency). Interestingly, the spurious band appearing at about 7.5 GHz in Fig. 4(a) does not appear in Fig. 8(a). i.e., the upper out-of-band response of the magnetically coupled structure is better than of the conventional one.

It has already been mentioned that the coupling between the resonators in the new configuration (DM operation) is magnetic in nature. This fact is illustrated by the high current density observed in the coupled sections of the resonators under DM excitation in Fig. 9(b). The magnetic coupling in this configuration is stronger than the electric coupling of the original configuration [see Fig. 9(a)]. Hence, the required gap for a given coupling level will be larger for the new configuration than for the electrically coupled resonators. However, for CM operation, the coupling mechanism is electric in both configurations, as it is qualitatively illustrated in Fig. 9(c) and (d). The key observation here is that the greater distance between the resonators allowed by the magnetically coupled configuration (DM operation) helps now to improve the CM rejection of the structure.

An interesting feature of the magnetically coupled structure is the appearance of an extra transmission zero (TZ) in the CM response (at approximately $f = 5.3$ GHz). This TZ is related to the difference in the modal phase velocities of the even and odd modes supported by the magnetically coupled sections as they behave as a pair of coupled microstrip lines [see Fig. 10(a)]. If this difference was zero, a passband would appear in the CM response in the frequency region above 5 GHz and below 6 GHz. Actually, the coupled section of length l_c is characterized by its even- and odd-mode characteristic impedances, Z_{0e}, Z_{0o}, respectively, and their even- and odd-mode electrical

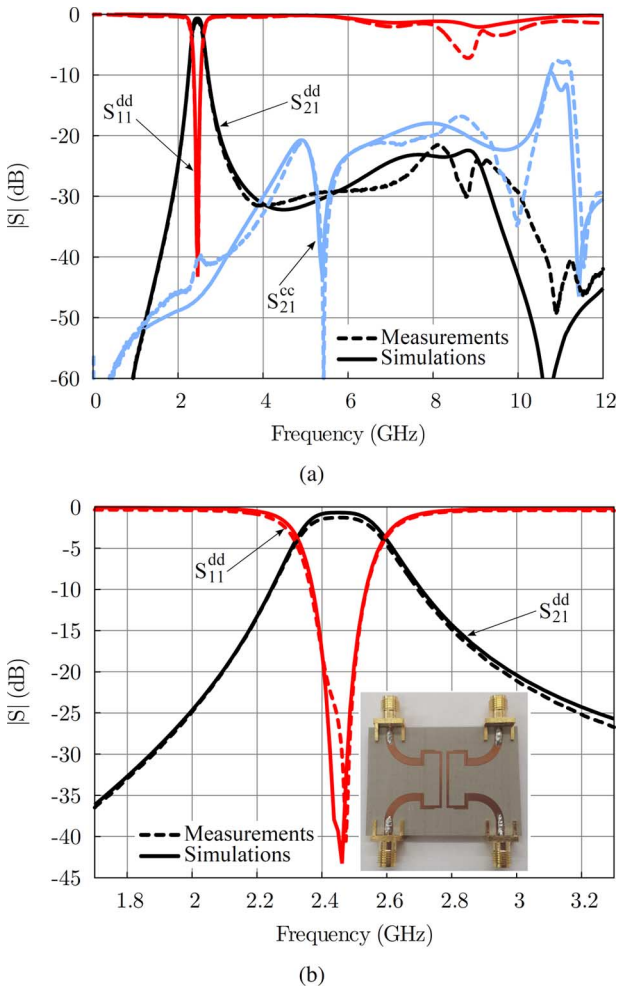

Fig. 8. (a) Simulated and measured DM and CM responses of the proposed open-loop balanced bandpass filter of Fig. 5. (b) Detail of the differential passband including a photograph of the prototype.

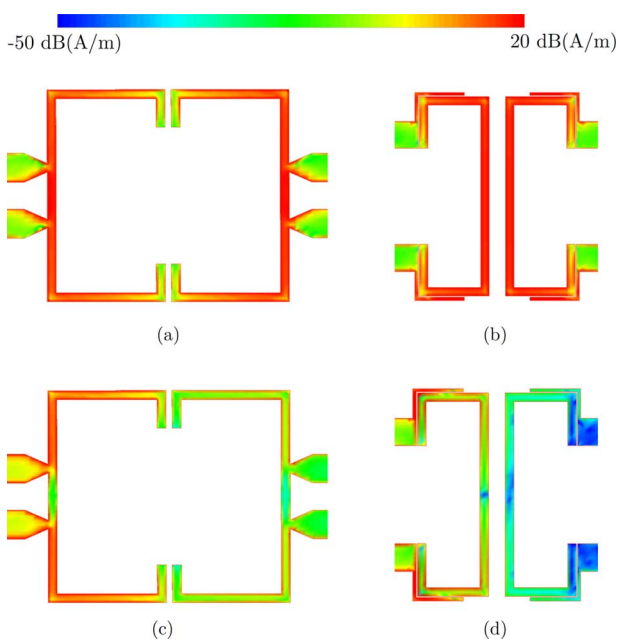

Fig. 9. Surface current distribution for DM (*top*) and CM (*bottom*) excitation of: (a) and (c) the electrically coupled and (b) and (d) the magnetically coupled configurations. Current patterns have been obtained at f_0^d.

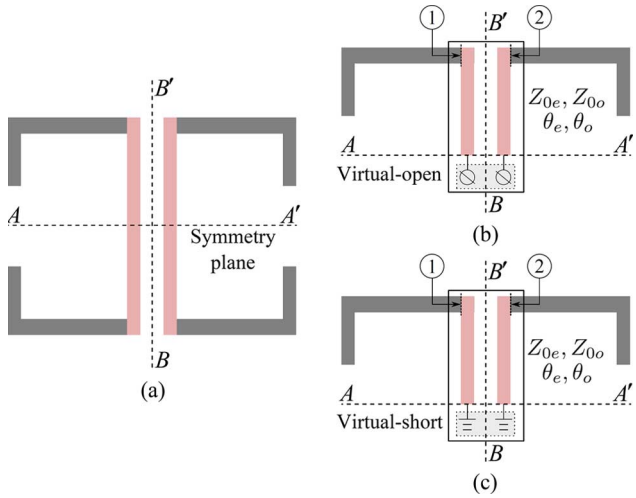

Fig. 10. (a) Basic structure of magnetically coupled $\lambda_g/2$-resonators. (b) CM equivalent half-circuit. (c) DM equivalent half-circuit.

lengths, θ_e, θ_o. The intrinsic response of this coupled microstrip section can be obtained by applying the even and odd excitation analysis [31, Ch.7] to the CM and DM equivalent circuits in Fig. 10(b) and (c). Taking into account the symmetry in the BB' plane, the following transmission coefficient, S_{21}, can be obtained:

$$S_{21} = \frac{1}{2}[S_{11}^{e} - S_{11}^{o}] \tag{4}$$

where S_{11}^{e} and S_{11}^{o} are the reflection coefficients for even and odd excitations. This results into the following expressions for CM and DM operation

$$S_{21}^{cc} = jZ_0 \frac{Z_{0o}\cot\theta_o - Z_{0e}\cot\theta_e}{(jZ_{0e}\cot\theta_e - Z_0)(jZ_{0o}\cot\theta_o - Z_0)} \tag{5}$$

$$S_{21}^{dd} = jZ_0 \frac{Z_{0o}\tan\theta_o - Z_{0e}\tan\theta_e}{(jZ_{0e}\tan\theta_e - Z_0)(jZ_{0o}\tan\theta_o - Z_0)}. \tag{6}$$

In the above formulas, $Z_0 = 25\ \Omega$ for CM and $Z_0 = 100\ \Omega$ for DM. The detailed application of this method, together with a study of the TZs of both responses and plots for S_{21}^{cc} and S_{21}^{dd} of the structures is provided in the Appendix. A simple inspection of the numerator in (5) reveals that the TZ in the CM response corresponds to a frequency f_{TZ} at which

$$Z_{0o}\cot\theta_o = Z_{0e}\cot\theta_e. \tag{7}$$

Note that if $\theta_e = \theta_o$ this TZ disappears. It can be demonstrated (see the Appendix) that, in the present filter, this occurs at $f_{TZ} = 5.3$ GHz, corresponding to values of θ_e and θ_o smaller than $\pi/2$. At this frequency, the coupling structure introduces the TZ observed in the CM response of our filter. Since this frequency depends on the electric parameters of the coupled region, they can be adjusted to make f_{TZ} coincide with the even resonance frequency of the open-loop resonator so that the undesired passband for the CM is partially eliminated. Fig. 11 shows the CM response of the magnetically coupled filter for different values of the length of the coupled section, $l_c = l_3/2$. The value of l_c has been modified while keeping the

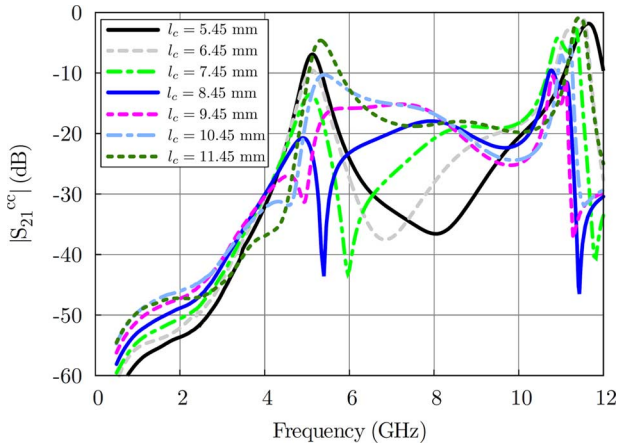

Fig. 11. Simulated CM response of several balanced bandpass filters based on magnetically coupled open-loop resonators for different values of l_c.

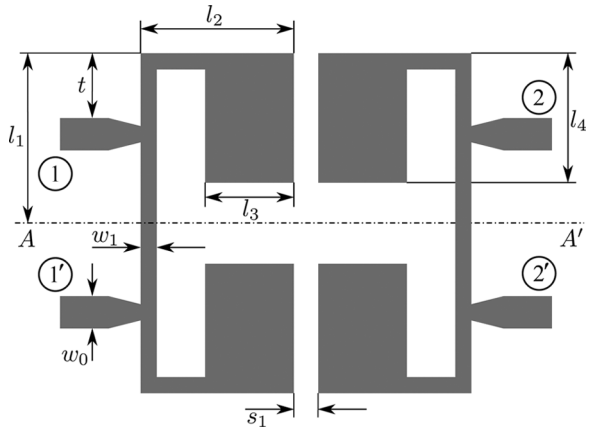

Fig. 12. Layout of a conventional balanced bandpass filter based on two electrically coupled FSIRs. The final dimensions of the designed filter are $l_1 = 7.05$ mm, $l_2 = 8.5$ mm, $l_3 = 4.4$ mm, $l_4 = 4.56$ mm, $w_0 = 2.53$ mm, $w_1 = 1$ mm, $t = 3.15$ mm, and $s_1 = 0.35$ mm.

total length of the resonator constant. From this plot, the dependence of the TZ on l_c is apparent; the longer the coupling region l_c, the lower the frequency of the TZ f_{TZ}. The best CM rejection is obtained for $l_c = 8.45$ mm, which was the value chosen for the filter presented in Fig. 8.

Summing up, the magnetically coupled configuration provides high in-band and good out-of-band CM rejection when compared with the electrically coupled version. The same concept can be used not only with open-loop resonators, but also with other types of resonators. In Section III, FSIRs, which are very popular for designing compact coupled-resonators filters, are employed to reduce the size of the filter and to achieve an extended good out-of-band performance also for the DM response.

III. Balanced Bandpass Filter Based on Electrically and Magnetically Coupled FSIRs

The use of FSIRs to design balanced differential bandpass filters has been reported, for instance, in [29] and [30]. As happens with differential filters based on open-loop resonators, electrical coupling of FSIRs also yields poor CM noise suppression. Again, lumped, distributed, or DGS elements can be added to the original design to enhance the CM response. However, it does not only increase the difficulty in the design process, but usually prevents the development of higher order filters due to the impossibility of cascading more than two resonators.

Next, it will be shown that the use of magnetic coupling provides a satisfactory CM response and also allows for the design of high-order filters. Fig. 12 shows the conventional topology of two electrically coupled FSIRs arranged to create a differential bandpass filter. The proposed arrangement with magnetic coupling is shown in Fig. 13. In order to compare the performance of both implementations, the same specifications and substrate are used for both of them: Butterworth prototype of order $n = 2$, center frequency $f_0^d = 2.45$ GHz, fractional bandwidth $\Delta = 10\%$, permittivity $\varepsilon_r = 3$, and thickness $h = 1.016$ mm. As already mentioned, the required coupling coefficient and external quality factor result to be $M_{12} = 0.071$ and $Q_e = 14$, respectively. Curves similar to those in Figs. 2, 3, 6, and Fig. 7 can

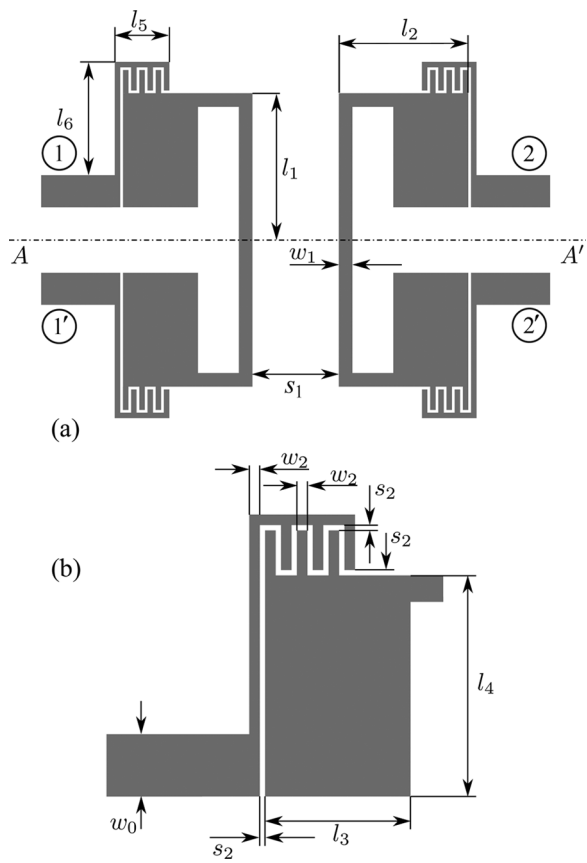

Fig. 13. (a) Layout of a novel balanced bandpass filter based on two magnetically coupled FSIRs and (b) a detail of the filter's feeding line. The final dimensions of the designed filter are $l_1 = 7.95$ mm, $l_2 = 5.45$ mm, $l_3 = 3.1$ mm, $l_4 = 4.26$ mm, $l_5 = 2.7$ mm, $l_6 = 3.03$ mm, $w_0 = 2.53$ mm, $w_1 = 0.8$ mm $w_2 = 3$ mm, $s_1 = 1.54$ mm, and $s_2 = 0.1$ mm.

be generated to obtain the physical dimensions that provide the required values of M_{12} and Q_e. In order to reach the required value of Q_e, an interdigitated capacitor has to be defined to excite the individual resonators, as is depicted in Fig. 13.

Numerical simulations and measured results for the two designed filters based on FSIRs (electrically or magnetically coupled) are shown in Figs. 14 and 15. These figures clearly show

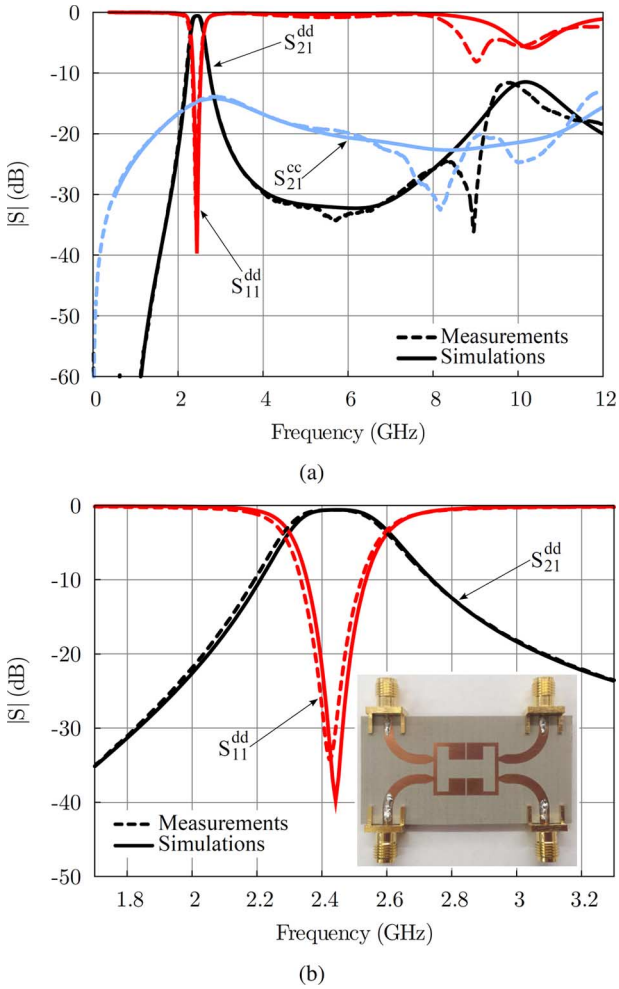

Fig. 14. (a) Simulated and measured DM and CM responses of the electrically coupled FSIRs balanced bandpass filter of Fig. 12. (b) Detail of the differential passband including a photograph of the fabricated prototype.

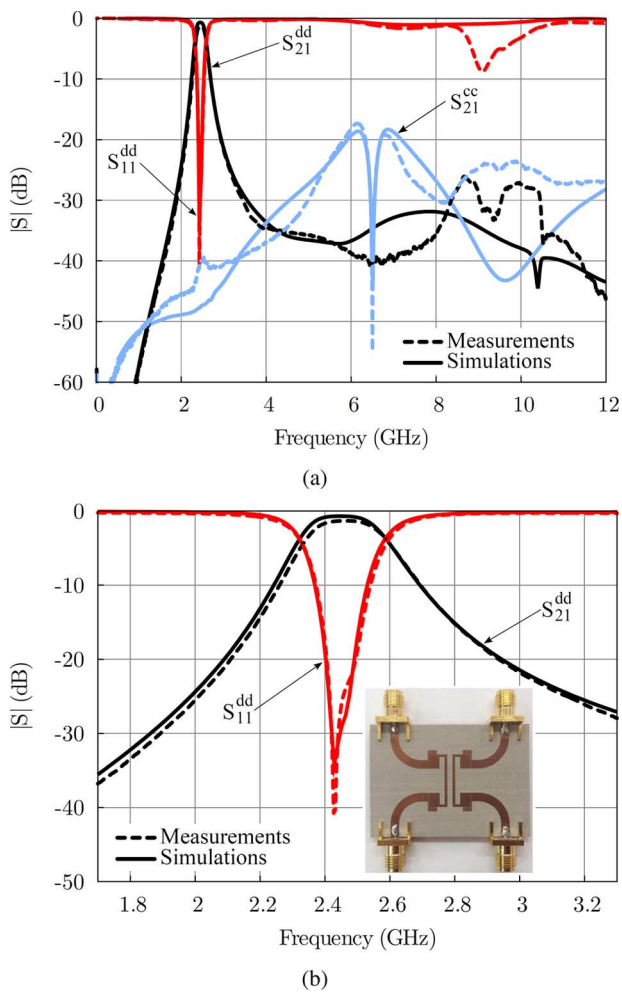

Fig. 15. (a) Simulated and measured DM and CM responses of the magnetically coupled FSIR balanced bandpass filter of Fig. 13. (b) Detail of the differential passband including a photograph of the prototype.

that CM suppression is drastically improved when magnetic coupling is employed. The measured CMRR ($@f_0^d$) achieved with the proposed magnetically coupled filter reaches 40 dB within the differential passband. Additionally, as it happened with the filter in Fig. 5, an extra TZ has been introduced in the CM response at 6.3 GHz, thus improving the CM performance even more. The out-of-band DM response is expected to be better for the FSIR based filters than for the open-loop based ones. This fact is observed in the response of the conventional electrically coupled filter ($|S_{21}^{dd}|$ is below -20 dB until 9 GHz, i.e., $3.7f_0^d$). However, the magnetically coupled FSIR filter presents an even better out-of-band performance, free of spurious passbands up to 12 GHz (about $5f_0^d$).

IV. Balanced Bandpass Filter Based on Magnetically Coupled FSIRs of Order $N = 4$

In previous sections, it has been shown that magnetic coupling can improve the CM performance of conventional electrically coupled resonators filters without degrading the DM response, which has been demonstrated with the implementation of filters of order $n = 2$. However, since the employed topology is quite simple (conventional resonators without any extra added elements), nothing prevents the application of this design procedure to higher order filters using an *inline* configuration. An increase in the number of resonators is expected to yield both better DM selectivity and CM suppression. This is not possible with many of the solutions usually found in the literature due to the complicated geometries that come into play, which make it unfeasible to build higher order filters in a straightforward way.

In this section, the methodology used previously for designing balanced bandpass filters of order $n = 2$ is extended to a filter of order $n = 4$. The layout of the proposed filter is depicted in Fig. 16. It should be pointed out that the size of the resonators 1 and 4 is different to that of resonators 2 and 3. As was already explained in Section II-B, the employed excitation (inductive/capacitive) affects the resonance frequency of the resonator. Hence, the dimensions of the resonators have to be adjusted to assure that the resonance frequency is the same for all the resonators that conform the filter. The chosen specifications for this new design are: Butterworth prototype, center frequency $f_0^d = 2.45$ GHz, and fractional bandwidth $\Delta = 14\%$ on a substrate of relative permittivity $\varepsilon_r = 3$ and thickness $h = 1.016$ mm. The required coupling coefficients and external

TABLE I
COMPARISON WITH REPORTED BALANCED BANDPASS FILTERS BASED ON COUPLED RESONATORS

	n	Size ($\lambda_g \times \lambda_g$)	Differential-mode				Common-mode	
			f_0^d (GHz)	3-dB Δ (%)	IL @f_0^d (dB)	$\Delta f_{3dB}/\Delta f_{20dB}$	CMRR @f_0^d (dB)	$\lvert S_{21}^{cc}\rvert$ (dB)
[20]	2	0.252 × 0.19	1.57	12.7	0.95	0.25	25	<-25 (0-2.3 GHz)
[32]	2	0.201 × 0.23	1.05	7	1.5	0.21	54.7	<-24 (0.5-3.5 GHz)
[33]	2	1.29 × 0.2	2.42	6.6	0.8	0.228	44	<-20 (0-4 GHz)
Fig. 5	2	0.195 × 0.246	2.455	11.1	1.28	0.316	38.8	<-30 (0-4.2 GHz)
Fig. 13	2	0.168 × 0.235	2.465	10.7	1.32	0.319	38.6	<-30 (0-5 GHz)
[30]	4	0.288 × 0.388	1.508	6	2.48	0.534	57	<-30 (0-14 GHz)
[29]	4	0.215 × 0.22	1.02	12	3.51	0.52	31	<-30 (0-6 GHz)
[14]	4	0.149 × 0.228	1.02	9.83	1.76	0.51	45	<-30 (0-6 GHz)
Fig. 16	4	0.373 × 0.214	2.475	13.9	1.105	0.528	47	<-30 (0-5.6 GHz)

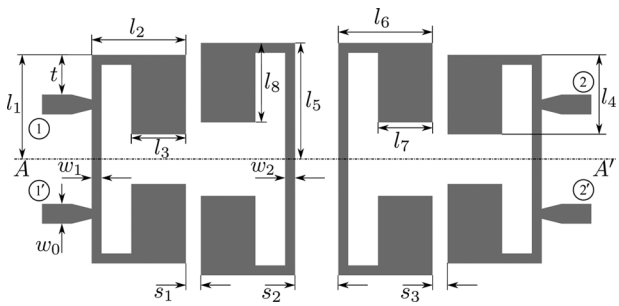

Fig. 16. Layout of a fourth-order balanced bandpass filter based on in-line coupled FSIRs. The final dimensions of the designed filter are (in millimeters): $l_1 = 8.4$, $l_2 = 7.32$, $l_3 = 2.98$, $l_4 = 4.86$, $l_5 = 8.7$, $l_6 = 6.35$, $l_7 = 3.1$, $l_8 = 4.26$, $w_0 = 2.53$, $w_1 = w_2 = 1$, $t = 2.93$, $s_1 = s_3 = 0.21$, and $s_2 = 1.54$.

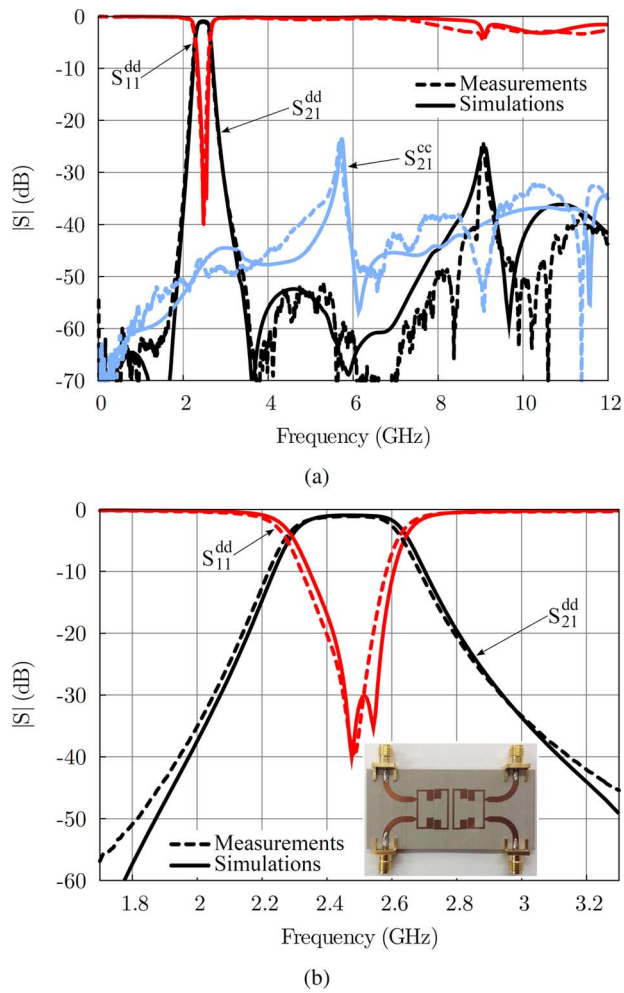

Fig. 17. (a) Simulated and measured DM and CM responses of the designed fourth-order FSIR balanced bandpass filter in Fig. 16. (b) Detail of the differential passband including a photograph of the fabricated prototype.

quality factors for the configuration in Fig. 16 can be obtained from (1) and (2), which are found to be $Q_{e1} = Q_{e4} = 5.47$, $M_{12} = M_{34} = 0.117$, and $M_{23} = 0.076$. Design curves for $M_{i,i+1}$ and Q_e similar to those of the previously designed filters can be generated using the full-wave simulator ADS Momentum. At this point it should be noted that two different curves for the coupling coefficient have to be obtained: one for the coupling between resonators 1 and 2 (3 and 4), which is mainly electric in nature, and another one for the coupling between resonators 2 and 3, which is mainly magnetic. Increasing the filter order results in a layout of resonators with alternating coupling schemes, thus ensuring the existence of at least a pair of magnetically coupled resonators in the filter. This magnetically coupled resonator pair is expected to highly improve the CM noise suppression. Additionally, due to the higher order of the filter, the selectivity of the DM response is also expected to be greatly improved.

All these observations are corroborated in Fig. 17, which shows the simulated and measured results for both DM and CM responses of the filter shown in Fig. 16. In this figure, a measured rejection level for CM of approximately 50 dB in the differential passband is observed, while measured IL is better than 1.2 dB in the passband. Furthermore, DM performance has been significantly improved in the out-of-band region since insertion IL is below -35 dB until 12 GHz and no spurious passbands are observed. As was predicted, the filter selectivity has been clearly improved and now the filter has steeper skirts. In addition to the good performance, this filter has been designed using a very well-known standard design procedure without any worry about CM rejection. Due to the nature of the magnetic coupling, the CM is automatically suppressed below -30 dB in the whole frequency band, except a peak of -24 dB at 5.67 GHz.

A comparison of the presented filters with previous solutions proposed in the literature is given in Table I. The new filters of order $n = 2$ of Figs. 5 and 13 are compared with similar structures of coupled resonators of the same order, where lumped

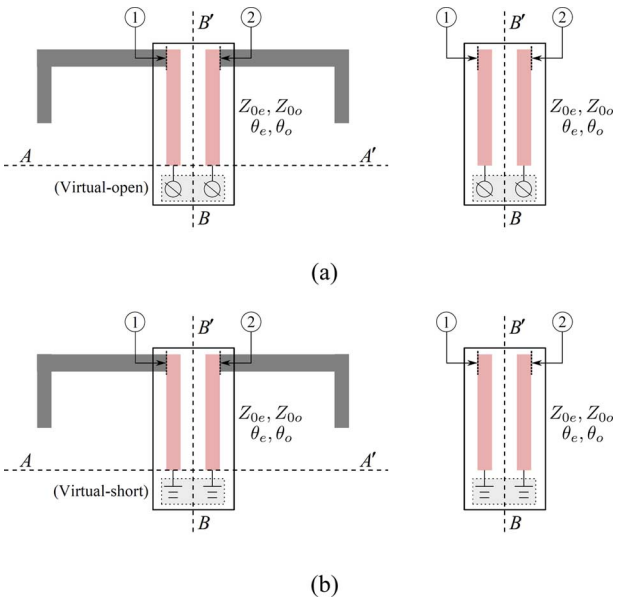

Fig. 18. Equivalent circuit and coupling structure under study for: (a) CM and (b) DM operation.

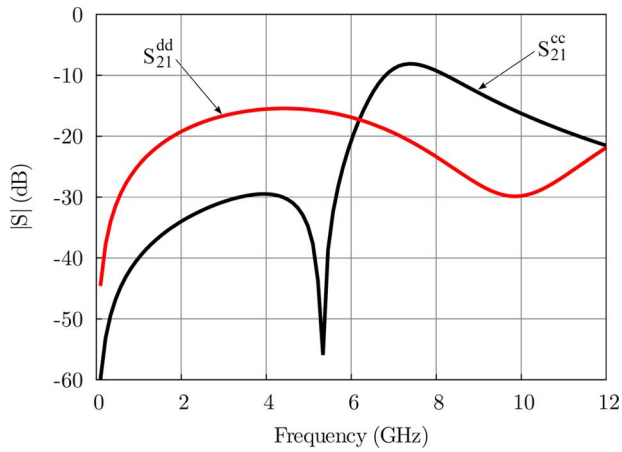

Fig. 19. Transmission coefficients for the structures under study represented in Fig. 18.

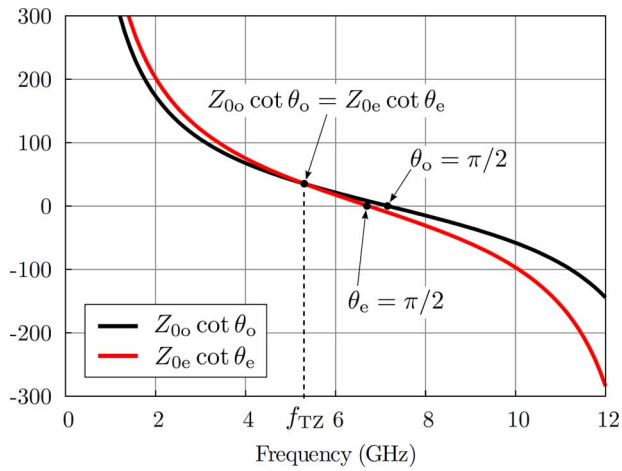

Fig. 20. Curves $Z_{0o}\cot\theta_o$ and $Z_{0e}\cot\theta_e$ versus frequency.

elements or DGSs have been used to improve CM rejection. It can be observed that the proposed novel filters provide a very good performance in terms of CM rejection with the additional advantage of having a continuous solid ground plane and no lumped elements. The filter of order $n = 4$ has also been compared with other similar filters, demonstrating a very competitive performance with the additional advantage of a simple design process. Moreover, it should be pointed out the flexibility that is obtained thanks to the possibility of implementing filters of any order in an *inline* configuration.

V. Conclusions

The symmetrically excited versions of coupled resonators filters based on open-loop or FSIR resonators behave as differential bandpass filters whose CM response is very different depending on the type of coupling between the resonators. It has been shown that magnetic coupling inherently leads to much better CM rejection without significant degradation of the DM response. This means that a good CM response can be obtained by using simple resonators without adding tuning elements for the CM response in the form of lumped/distributed components or DGS structures. This fact significantly simplifies the design procedure and reduces the need for fine tuning based on time-consuming numerical optimization. Moreover, high-order filters with very good CM rejection can easily be designed thanks to the existence of magnetically coupled sections embedded in them.

Appendix

In this Appendix, the analysis of the coupling structure proposed in Section II-B is carried out by means of equivalent circuits for CM and DM operation. The structure is basically a pair of symmetrical coupled lines with different boundary conditions depending on the excitation (even or odd), as shown in Fig. 18. Due to the symmetry with respect to the BB' plane, the even and odd excitation analysis can be used to obtain the transmission coefficient, S_{21}, for the structures under study as

$$S_{21} = \frac{1}{2}[S_{11}^{e} - S_{11}^{o}]. \tag{8}$$

Under CM excitation, the AA' plane behaves as a virtual open-circuit, resulting in the circuit in Fig. 18(a). The virtual open can be translated to the input port to obtain the following reflection coefficient for the even and odd excitations:

$$S_{11}^{e} = \frac{-jZ_{0e}\cot\theta_e - Z_0}{-jZ_{0e}\cot\theta_e + Z_0} \tag{9}$$

$$S_{11}^{o} = \frac{-jZ_{0o}\cot\theta_o - Z_0}{-jZ_{0o}\cot\theta_o + Z_0} \tag{10}$$

where Z_{0e} and Z_{0o} are the even- and odd-mode characteristic impedances of the coupled lines, Z_0 is the characteristic impedance of the system (25 Ω in this case), and finally, θ_e and θ_o are the electrical lengths of the even and odd modes, respectively.

Using (8), the transmission coefficient of the structure is given by

$$S_{21}^{cc} = jZ_0\frac{Z_{0o}\cot\theta_o - Z_{0e}\cot\theta_e}{(jZ_{0e}\cot\theta_e - Z_0)(jZ_{0o}\cot\theta_o - Z_0)}. \tag{11}$$

Under DM excitation, the AA' plane behaves as a virtual short-circuit, resulting in the circuit in Fig. 18(b). The virtual short can be translated to the input port and the reflection coefficient can be calculated for the even and odd excitations as follows:

$$S_{11}^{\mathrm{e}} = \frac{jZ_{0\mathrm{e}}\tan\theta_{\mathrm{e}} - Z_0}{jZ_{0\mathrm{e}}\tan\theta_{\mathrm{e}} + Z_0} \tag{12}$$

$$S_{11}^{\mathrm{o}} = \frac{jZ_{0\mathrm{o}}\tan\theta_{\mathrm{o}} - Z_0}{jZ_{0\mathrm{o}}\tan\theta_{\mathrm{o}} + Z_0} \tag{13}$$

with $Z_0 = 100\ \Omega$ in this case.

Again, applying (8), the following transmission coefficient for the DM is obtained:

$$S_{21}^{\mathrm{dd}} = jZ_0 \frac{Z_{0\mathrm{e}}\tan\theta_{\mathrm{e}} - Z_{0\mathrm{o}}\tan\theta_{\mathrm{o}}}{(jZ_{0\mathrm{e}}\tan\theta_{\mathrm{e}} + Z_0)(jZ_{0\mathrm{o}}\tan\theta_{\mathrm{o}} + Z_0)}. \tag{14}$$

The expressions (11) and (14), which describe the behavior of the coupling structure of the new filter under CM and DM excitation, are plotted in Fig. 19 versus frequency. The TZs present in the CM response can easily be analyzed using (11). In an homogeneous medium where $\theta_{\mathrm{e}} = \theta_{\mathrm{o}}$, the zero will occur when $\cot\theta_{\mathrm{e}} = \cot\theta_{\mathrm{o}} = 0$, namely, when $\theta_{\mathrm{e}} = \theta_{\mathrm{o}} = \pi/2$. However, for a inhomogeneous medium where $\theta_{\mathrm{e}} \neq \theta_{\mathrm{o}}$ (as is the case for microstrip technology), the TZ will correspond to the frequency f_{TZ} at which $Z_{0\mathrm{o}}\cot\theta_{\mathrm{o}} = Z_{0\mathrm{e}}\cot\theta_{\mathrm{e}}$. This frequency can be graphically obtained by plotting the behavior of both members of the above equation and finding the crossing point, as shown in Fig. 20. It should be noted that this frequency corresponds to values of θ_{e} and θ_{o} lower than $\pi/2$. Another trivial zero is found when $\theta_{\mathrm{e}} = \theta_{\mathrm{o}} = 0$ for both homogeneous and inhomogeneous structures (this occurs at $f_{\mathrm{TZ}} = 0$ GHz).

A similar analysis can be applied to the transmission coefficient of the DM given in (14). For the homogeneous case ($\theta_{\mathrm{e}} = \theta_{\mathrm{o}}$), TZs would occur when $\theta_{\mathrm{e}} = \theta_{\mathrm{o}} = 0$, π, or $\pi/2$. However, for our present case of inhomogeneous medium ($\theta_{\mathrm{e}} \neq \theta_{\mathrm{o}}$), a TZ is present only when $\theta_{\mathrm{e}} = \theta_{\mathrm{o}} = 0$. The absence of DM TZs different from $f_{\mathrm{TZ}} = 0$ GHz is depicted in Fig. 19.

REFERENCES

[1] W. R. Eisenstant, B. Stengel, and B. M. Thompson, *Microwave Differential Circuit Design Using Mixed-Mode S-Parameters*. Boston, MA, USA: Artech House, 2006.

[2] B. Xia, L.-S. Wu, and J.-F. Mao, "A new balanced-to-balanced power divider/combiner," *IEEE Trans. Microw. Theory Techn.*, vol. 60, no. 9, pp. 2791–2798, Sep. 2012.

[3] B. Xia, L.-S. Wu, S.-W. Ren, and J.-F. Mao, "A balanced-to-balanced power divider with arbitrary power division," *IEEE Trans. Microw. Theory Techn.*, vol. 61, no. 8, pp. 2831–2840, Aug. 2013.

[4] L.-S. Wu, Y.-X. Guo, and J.-F. Mao, "Balanced-to-balanced gysel power divider with bandpass filtering response," *IEEE Trans. Microw. Theory Techn.*, vol. 61, no. 12, pp. 4052–4062, Dec. 2013.

[5] W. Feng, H. Zhu, W. Che, and Q. Xue, "Wideband in-phase and out-of-phase balanced power dividing and combining networks," *IEEE Trans. Microw. Theory Techn.*, vol. 62, no. 5, pp. 1192–1202, May 2014.

[6] Y. Zhou, H.-W. Deng, and Y. Zhao, "Compact balanced-to-balanced microstrip diplexer with high isolation and common-mode suppression," *IEEE Microw. Wireless Compon. Lett.*, vol. 24, no. 3, pp. 143–145, Mar. 2014.

[7] C.-Y. Hsiao and T.-L. Wu, "A novel dual-function circuit combining high-speed differential equalizer and common-mode filter with an additional zero," *IEEE Microw. Wireless Compon. Lett.*, vol. 24, no. 9, pp. 617–619, Sep. 2014.

[8] T.-W. Weng, C.-H. Tsai, C.-H. Chen, D.-H. Han, and T.-L. Wu, "Synthesis model and design of a common-mode bandstop filter (CM-BSF) with an all-pass characteristic for high-speed differential signals," *IEEE Trans. Microw. Theory Techn.*, vol. 62, no. 8, pp. 1647–1656, Aug. 2014.

[9] S.-J. Wu, C.-H. Tsai, T.-L. Wu, and T. Itoh, "A novel wideband common-mode suppression filter for GHz differential signals using coupled patterned ground structure," *IEEE Trans. Microw. Theory Techn.*, vol. 57, no. 4, pp. 848–855, Apr. 2009.

[10] F. de Paulis, L. Raimondo, S. Connor, B. Archambeault, and A. Orlandi, "Compact configuration for common mode filter design based on planar electromagnetic bandgap structures," *IEEE Trans. Electromagn. Compat.*, vol. 54, no. 3, pp. 646–654, Jun. 2012.

[11] J. Naqui *et al.*, "Common mode suppression in microstrip differential lines by means of complementary split ring resonators: Theory and applications," *IEEE Trans. Microw. Theory Techn.*, vol. 60, no. 10, pp. 3023–3034, Oct. 2012.

[12] A. Fernández-Prieto *et al.*, "Dual-band differential filter using broadband common-mode rejection artificial transmission line," *Progr. Electromagn. Res.*, vol. 139, pp. 779–797, Apr. 2013.

[13] G.-H. Shiue, C.-M. Hsu, C.-L. Yeh, and C.-F. Hsu, "A comprehensive investigation of a common-mode filter for gigahertz differential signals using quarter-wavelength resonators," *IEEE Trans. Compon., Packag., Manuf. Technol.*, vol. 4, no. 1, pp. 134–144, Jan. 2014.

[14] J.-L. Olvera-Cervantes and A. Corona-Chávez, "Microstrip balanced bandpass filter with compact size, extended-stopband and common-mode noise suppression," *IEEE Microw. Wireless Compon. Lett.*, vol. 23, no. 10, pp. 530–532, Oct. 2013.

[15] Y.-H. Cho and S.-W. Yun, "Design of balanced dual-band bandpass filters using asymmetrical coupled lines," *IEEE Trans. Microw. Theory Techn.*, vol. 61, no. 8, pp. 2814–2820, Aug. 2013.

[16] A. K. Horestani, M. Durán-Sindreu, J. Naqui, C. Fumeaux, and F. Martin, "S-shaped complementary split ring resonators and their application to compact differential bandpass filters with common-mode suppression," *IEEE Microw. Wireless Compon. Lett.*, vol. 24, no. 3, pp. 149–151, Mar. 2014.

[17] X.-H. Wu, Q.-X. Chu, and L.-L. Qiu, "Differential wideband bandpass filter with high-selectivity and common-mode suppression," *IEEE Microw. Wireless Compon. Lett.*, vol. 23, no. 12, pp. 644–646, Dec. 2013.

[18] L. Li, J. Bao, J.-J. Du, and Y.-M. Wang, "Differential wideband bandpass filters with enhanced common-mode suppression using internal coupling technique," *IEEE Microw. Wireless Compon. Lett.*, vol. 24, no. 5, pp. 300–302, May 2014.

[19] X. Xu, J. Wang, and L. Zhu, "A new approach to design differential-mode bandpass filters on SIW structure," *IEEE Microw. Wireless Compon. Lett.*, vol. 23, no. 12, pp. 635–637, Dec. 2013.

[20] J. Shi and Q. Xue, "Balanced bandpass filters using center-loaded half-wavelength resonators," *IEEE Trans. Microw. Theory Techn.*, vol. 58, no. 4, pp. 970–977, Apr. 2010.

[21] W. Feng and W. Che, "Novel wideband differential bandpass filters based on T-shaped structure," *IEEE Trans. Microw. Theory Techn.*, vol. 60, no. 6, pp. 1560–1568, Jun. 2012.

[22] X.-H. Wu and Q.-X. Chu, "Compact differential ultra-wideband bandpass filter with common-mode suppression," *IEEE Microw. Wireless Compon. Lett.*, vol. 22, no. 9, pp. 456–458, Sep. 2012.

[23] Y.-J. Lu, S.-Y. Chen, and P. Hsu, "A differential-mode wideband bandpass filter with enhanced common-mode suppression using slotline resonator," *IEEE Microw. Wireless Compon. Lett.*, vol. 22, no. 10, pp. 503–505, Oct. 2012.

[24] P. Vélez *et al.*, "Differential bandpass filter with common-mode suppression based on open split ring resonators and open complementary split ring resonators," *IEEE Microw. Wireless Compon. Lett.*, vol. 23, no. 1, pp. 22–24, Jan. 2013.

[25] W. Feng, W. Che, Y. Ma, and Q. Xue, "Compact wideband differential bandpass filters using half-wavelength ring resonator," *IEEE Microw. Wireless Compon. Lett.*, vol. 23, no. 2, pp. 81–83, Feb. 2013.

[26] J. Shi *et al.*, "Compact low-loss wideband differential bandpass filter with high common-mode suppression," *IEEE Microw. Wireless Compon. Lett.*, vol. 23, no. 9, pp. 480–482, Sep. 2013.

[27] J.-S. Hong, *Microstrip Filters for RF/Microwave Applications*, 2nd ed. New York, NY, USA: Wiley, 2011.

[28] ADS-Momentum. Keysight Technol., Santa Rosa, CA, USA, 2015. [Online]. Available: http://www.keysight.com/

[29] C.-H. Wu, C.-H. Wang, and C. H. Chen, "Stopband-extended balanced bandpass filter using coupled stepped-impedance resonators," *IEEE Microw. Wireless Compon. Lett.*, vol. 17, no. 7, pp. 507–509, Jul. 2007.
[30] S.-C. Lin and C.-Y. Yeh, "Stopband-extended balanced filters using both $\lambda/4$ and $\lambda/2$ SIRs with common-mode suppression and improved passband selectivity," *Progr. Electromagn. Res.*, vol. 128, pp. 215–228, May 2012.
[31] D. M. Pozar, *Microwave Engineering*, 4th ed. Hoboken, NJ, USA: Wiley, 2012.
[32] J. Shi, J. Chen, H. Tang, and L. Zhou, "Differential bandpass filter with high common-mode rejection ratio inside the differential-mode passband using controllable common-mode transmission zero," in *IEEE Int. Wireless Symp.*, Beijing, China, Apr. 2013, 4 pp.
[33] H. Wang, K.-W. Tam, S.-K. Ho, W. Kang, and W. Wu, "Short-ended self-coupled ring resonator and its application for balanced filter design," *IEEE Microw. Wireless Compon. Lett.*, vol. 24, no. 5, pp. 312–314, May 2014.

Armando Fernández-Prieto was born in Ceuta, Spain, in September 1981. He received the Licenciado and Ph.D. degrees in physics from the University of Seville, Seville, Spain, in 2007 and 2013, respectively.

He is currently involved with post-doctoral research with the Microwaves Group, University of Seville. His research interests focus on printed passive microwave filters, couplers, and metamaterials.

Dr. Fernández-Prieto is a reviewer for the IEEE TRANSACTIONS ON MICROWAVE THEORY AND TECHNIQUES, as well as for many other journals.

Aintzane Lujambio was born in San Sebastián (Guipúzcoa), Spain, in 1982. She received the Telecommunication Engineering degree and Ph.D. degree in communication technologies from the Public University of Navarre, Navarre, Spain, in 2006 and 2014, respectively.

She has worked with the Microwaves Group, University of Seville. She has collaborated on several research projects supported by the Spanish Government and the European Commission. Her research interests include algorithms for microwave applications, inverse-scattering synthesis methods, passive microwave filters, and couplers.

Jesús Martel (M'08–SM'15) received the Licenciado and Doctor degrees in physics from the University of Seville, Seville, Spain, in 1989 and 1996, respectively.

Since 1990, he has performed research with the Microwave Group, University of Seville. In 1992, he joined the Department of Applied Physics II, University of Seville, where, in 2000, he became an Associate Professor, and in 2010, Head of the department. His current research interest is focused on the numerical analysis of planar transmission lines, the modeling of planar microstrip discontinuities, the design of passive microwave circuits, microwave measurements, and artificial media.

Francisco Medina (M'90–SM'01–F'10) was born in Puerto Real, Cádiz, Spain, in November 1960. He received the Licenciado and Doctor degrees in physics from the University of Seville, Seville, Spain, in 1983 and 1987 respectively.

He is currently a Professor of electromagnetism with the Department of Electronics and Electromagnetism, University of Seville, and Head of the Microwaves Group. He has coauthored more than 135 journal papers and book chapters, as well as more than 270 conference contributions. He is member of the Editorial Board of three technical journals. His research interests include analytical and numerical methods for planar structures, anisotropic materials, and artificial media modeling.

Prof. Medina is a reviewer for about 45 IEEE, IET, AIP, and IoP journals. He has been member of the Technical Program Committees (TPCs) of a number of local and international leading conferences.

Francisco Mesa (M'93–SM'11–F'14) was born in Cádiz, Spain, in April 1965. He received the Licenciado and Doctor degrees in physics from the Universidad de Sevilla, Seville, Spain, in 1989 and 1991, respectively.

He is currently a Professor with the Departamento de Física Aplicada 1, Universidad de Sevilla, Seville, Spain. His research interests focus on electromagnetic propagation/radiation in planar structures.

Rafael R. Boix (M'96) received the Licenciado and Doctor degrees in physics from the University of Seville, Seville, Spain, in 1985 and 1990, respectively.

Since 1986, he has been with the Electronics and Electromagnetism Department, University of Seville, where he became a Tenured Professor in 2010. His current research interests focus on the efficient numerical analysis of periodic planar multilayered structures with applications to the design of frequency-selective surfaces and reflectarray/transmitarray antennas.